Acker, J., T. Sieber, and V. Hoffmann. 2026. Copper Impurities in Silicon Kerf. In *Silicon for the chemical and solar industry XVIII*, edited by M. Tangstad, H. Rong, A. Valderhaug, B. Andresen, H. Dalaker, and I. G. Page. Kristiansand, Norway, September 7–10, 2026.
https://doi.org/10.55669/oa900815

Copper Impurities in Silicon Kerf

J. Acker, T. Sieber, and V. Hoffmann
Brandenburg Technical University Cottbus-Senftenberg,
Department of Physical Chemistry, D-01968 Senftenberg, Germany,
joerg.acker@b-tu.de

Keywords: kerf, copper, GD-OES, acidic treatment

Abstract Silicon wafers are manufactured using wire sawing processes, during which a significant portion—approximately 35–40%—of the high-purity silicon is lost in the form of very fine particles known as "Kerf." An economically meaningful use of kerf is only possible if the metallic impurities introduced during sawing can be efficiently removed. Copper poses a particular challenge in this context, as it creates deep defects in silicon, preventing it from being reused as a semiconductor material without additional processing steps. This study examines the mechanism by which copper is introduced into the kerf and outlines the challenges involved when attempting to reduce the concentration of copper in the kerf through wet chemical etching processes.

1. INTRODUCTION

Sawing silicon wafers results in significant material loss, which is referred to as "kerf loss" or simply "kerf." The kerf is a material of economic importance, particularly in the photovoltaic and semiconductor industries, since wire sawing typically results in the loss of about 35–40% of the original silicon ingot made of high-purity silicon as sawing slurry (Würzner *et al.*, 2014).

A method of wafer sawing is the slurry process, in which a steel wire is used together with a suspension of abrasive silicon carbide particles (loose abrasive slurry sawing). Material removal from the silicon is achieved through fracture formation processes, whereby the steel wire presses sharp-edged silicon carbide particles onto the silicon block (Möller, 2004). The kerf consists of fine silicon particles with particle sizes mostly under 10 µm and contains the more or less ground-down and fractured SiC particles, furthermore steel particles resulting from direct abrasion of the steel wire as well as adhering residues of coolants and lubricants.

Modern solar wafer production lines predominantly use diamond wire saws in which diamond grains are permanently bonded to a wire (fixed abrasive diamond wire sawing). This technology enables higher cutting speeds and lower material loss (Kumar and Melkote, 2018; *Li et al.*, 2023). In this technology, it is the diamond particles adhering directly to the wire that transfer the mechanical forces exerted by the wire to the silicon, thereby triggering the fracture processes in the silicon block. Consequently, the kerf contains nickel and iron contaminants from the abraded steel particles. The diamond particles can be fixed to the steel wire using organic resins or brass or nickel alloys, and latter leads to the introduction of copper, zinc and nickel into the kerf. Consequently, the type and concentration of metallic contaminants in the kerf depend heavily on the saw wire used and can range from a few ppm to several thousand ppm of total metallic impurity (Lottspeich *et al.*, 2018; Kong *et al.*, 2019; Xiong *et al.*, 2024).

A variety of process variants have been developed for silicon recovery; details of these can be found in the relevant literature (Li *et al.*, 2021; Xiong *et al.*, 2024). The core element of every

processing method is the removal of metallic contaminants using inorganic acids, such as sulfuric acid (H_2SO_4), hydrochloric acid (HCl), nitric acid (HNO_3), and hydrofluoric acid (HF), which may be followed by various further processing steps.

2. RESULTS

2.1 Experimental

Table 1 shows the composition of the used kerf and silicon purity calculated from the impurity elements listed in the table. Other impurities include: Cr < 0.4 ppm, Mn < 0.5 ppm, Co < 0.6 ppm, as well as B at 1.65 ppm and P at 16.16 ppm, which are insignificant in the chemical treatment (Cr, Mn, Co) or undergo no significant change (B, P). Iron, nickel, copper, and zinc are the most significant impurities and represent the abrasion on both the steel wire and the brass alloy. Impurities from aluminum, calcium, and magnesium are primarily introduced by the process media during sawing and in the post-treatment of the kerf in the collection tanks.

For chemical treatment, several grams of kerf were suspended in the respective acid or acid mixture at room temperature and stirred continuously for 60 minutes at a stirring speed of approximately 500 rpm. In all experiments, a mass-based solid-to-liquid ratio of 20% was selected, with a typical solution volume of approximately 50 mL. The treated kerf was separated by vacuum filtration, washed several times with deionized water, and gently dried. The initial samples as well as the purified samples were dissolved in a mixture of HF-HNO_3 and subsequently analyzed by ICP-OES (Rietig and Acker, 2017).

All impurity concentrations are expressed in mass ppm, based on the initial weight of the sample. The acid concentrations in mass percent (% (m/m)) are based on the proportions of concentrated acid prepared from the respective concentrated acids (HNO_3 65% (v/v), HF 40% (v/v), and HCl 30% (v/v), all acids are Suprapur).

Table I: Composition of the kerf as starting material and at the maximum purity achieved after a three-step treatment process in the sequence 30% HNO_3 – 4% HF – 30% HCl.

	Element impurity content [ppm]									silicon content [%]
	Al	Fe	Ca	Mg	Cu	Ni	Zn	Ti	sum	
kerf as-received	4813.5	94.6	158.9	39.2	11.3	415.1	13.71	1.3	5547.5	99.445
kerf leached	9.5	13.1	1.2	5.4	5.0	6.0	0.8	0.3	41.3	99.996

ICP-OES measurements were performed using an iCap 6500 DUO (Thermo Scientifc, Germany) with a dual-view option and equipped with an HF-resistant sample introduction system with a parallel path nebuliser made of PEEK (MiraMist, Burgener Inc.), a cyclonic chamber made of PTFE (Glass Expansion) and a ceramic injector tube (Glass Expansion).

A commercial GD-OES instrument GDS 750 (Spectruma, Hof, Germany) with PMT detection was used in HF mode. This instrument is also equipped with a monochromator (DigiKröm 480, Spectral Products, Albuquerque, USA) with a range of 200–750 nm.

2.2 Selection of an Etching Regime

Three different acids were selected for treating the kerf. Due to its high oxidation potential, nitric acid is capable of dissolving most metallic impurities, including copper; however, it causes surface passivation, particularly on steel alloys. Hydrochloric acid, as a non-oxidizing acid, also dissolves many metallic impurities and does not cause passivation. It can be assumed that the kerf particles are surrounded by a thin oxide layer, which under sawing conditions (aqueous medium, metallic impurities, oxygen) can reach a higher thickness than the known native oxide layer of silicon. Metallic impurities are usually protected from attack by HCl and HNO_3 as long as they are located within or below the oxide layer and as long as the oxide layer does not exhibit particularly high porosity. To remove this oxide layer, treatment with hydrofluoric acid (HF) solutions is required. In addition, hydrofluoric acid-hydrochloric acid mixtures (HF/HCl) were tested to combine the removal of the oxide layer from the kerf particles with the high solubility for metals. Hydrofluoric acid-nitric acid mixtures were not used, as these lead to the complete dissolution of the silicon particles.

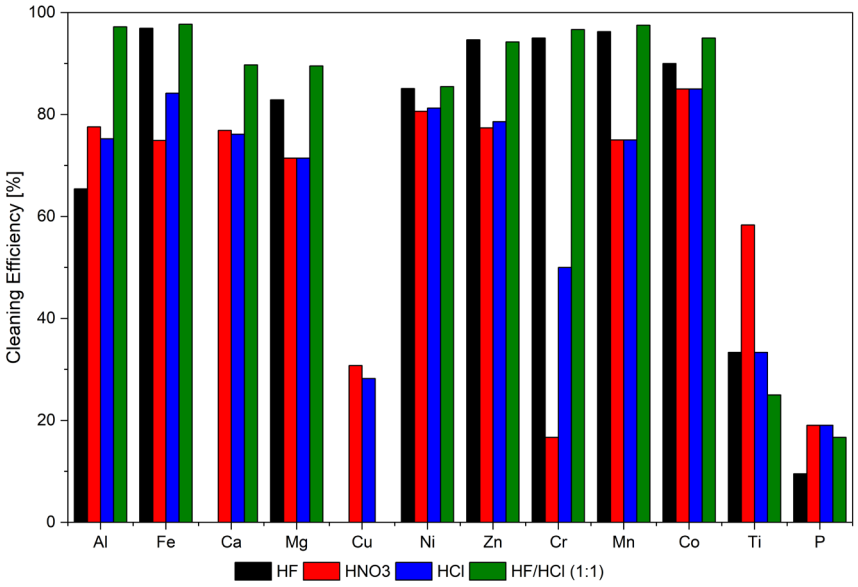

Figure 1: Kerf cleaning efficiency using four different etching regimens.

As Figure 1 shows, the HF-HCl mixture results in the highest removal of metallic impurities when considering all elements, which is significantly higher than what could be achieved with HNO_3 or HCl alone. This suggests that a certain amount of the impurities is protected within or beneath the oxide layer and is largely shielded from surface acid attack. Further investigations show that this dissolution behavior can be further optimized by varying the HF-to-HCl mixing ratios and by adjusting the total concentration of the acids. However, these positive findings do not apply to copper. Only HNO_3 and HCl (when the solution is stirred, allowing atmospheric oxygen to enter) are capable of reducing the copper content at all. It should be noted, that in all studies in which HF/HCl mixtures were used, the final copper content corresponded to the initial value or even slightly exceeded it. This effect of re-deposition will be discussed later.

2.3 On the interaction between copper and silicon

The behavior of copper raises questions about its presence in the kerf and its fate in the acid solution. Because some of the copper can be dissolved by HNO_3, it can be assumed that only individual copper particles or copper adhering to the surface of the silicon particles is accessible to the acid. It cannot be determined whether this copper consists exclusively of

metallic copper or also includes partially oxidized copper particles. Even in an HCl-acid solution, metallic copper can dissolve in small quantities if sufficient atmospheric oxygen is introduced into the solution, for example during stirring. Furthermore, if hydrofluoric acid enables the dissolution and complexation of silicon, this opens the reaction pathway for the electrochemical deposition of copper on the silicon as $[SiF_6^{2-}]$-ions, a process widely known as metal-assisted etching (Schönekerl and Acker 2020). Deposition can only be prevented in presence of a strong oxidizing agent (e.g., hydrogen peroxide, potassium peroxodisulfate), however, the use of which was not planned within the scope of this work.

Of greater importance is the fraction of copper that cannot be removed by the acid treatment. In this respect, a hypothesis was developed that the high mechanical forces generated during diamond wire sawing—specifically at the points of contact between the brass-coated sections of the wire and the silicon surface, or with already abraded silicon particles, lead to the penetration of copper into the silicon.

To verify these hypotheses, the surfaces of polished single-crystal wafer pieces were treated once using a diamond grinder, in which the diamond particles were bound to the steel wheel with an organic resin adhesive, and once with a brass grinding attachment. These mechanical treatments were performed once dry and once with an aqueous, diluted $CuSO_4$ solution. In parallel, wafer pieces were immersed in an aqueous, HF-free, diluted $CuSO_4$ solution to simulate copper penetration without mechanical stress. After completion, all wafer pieces were treated with an aqueous ammonium peroxodisulfate solution, to dissolving metallic copper particles and copper silicide phases; copper diffused into the silicon is not dissolved.

Using GD-OES (glow discharge optical emission spectroscopy), the depth profile of copper penetration into the silicon can be determined. In GD-OES the measured intensity of an element emission line is proportional to the partial pressure of the element in the plasma, and under stable plasma conditions this is proportional to the element concentration in the solid. However, the calibration of the copper emission intensity was omitted, so that quantification of the copper content is not possible. Calibration of the erosion depth was also omitted, and the depth of erosion is instead specified as time of sputtering. For a qualitative assessment, it is entirely sufficient to examine the profile of copper emission intensity in relation to the profile of silicon emission intensity as the main component. GD-OES spectra are characterized by a "start-up effect" of the plasma lasting several milliseconds, during which the intensities of the sputtered elements initially build up over time. Surfaces of solids are always contaminated by thin oxide layers, organic deposits, and adsorbed water and CO_2, these are abruptly released upon plasma ignition. Since the emission intensities of any elements are proportional to their corresponding partial pressure in the sputtering chamber including the elements released from the desorbed surface impurities, a quantification of the analyte elements is not possible during this "start-up" period.

The analyses show that a simple immersion of silicon wafers in a HF free, diluted copper salt solution does not lead to a diffusion of copper into silicon; no copper signal is detectable by GD-OES. If the surface is treated with a resin-bonded diamond disc in the presence of a copper salt solution, only a larger fluctuation in the very low copper signal is observed, which also does not account for a significant diffusion of copper into the silicon.

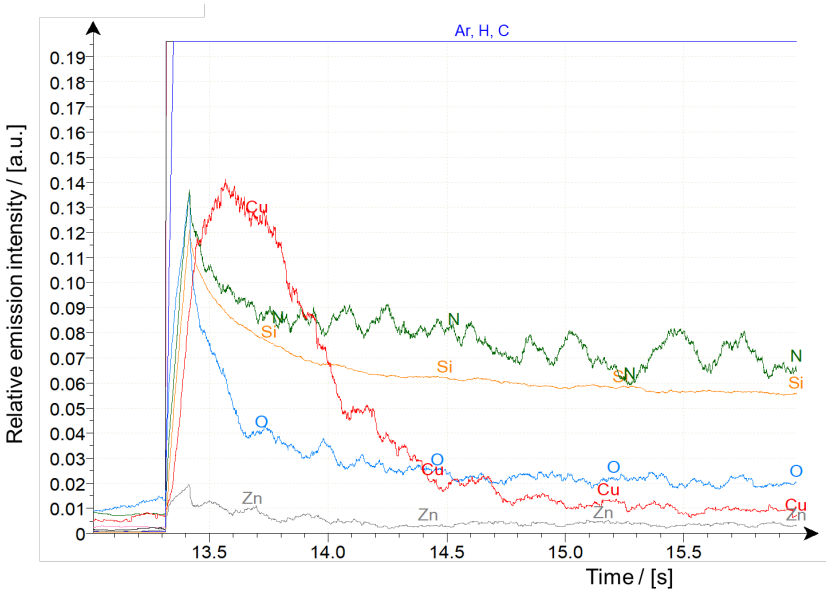

Figure 2: GD-OES depth profile analysis for a Si wafer that was dry-polished using a brass polishing wheel.

Figure 2 shows the depth profile of copper in silicon (along with Zn, O, N, and Si) following dry polishing with a brass polishing wheel. The profile of copper emission intensity shows a high emission intensity that decrease only slowly with increasing depth, i.e., over long erosion times of approximately 1.5 seconds. Zinc is also present in the near-surface region, and elevated levels of oxygen are detectable, indicating oxidation in the nearby surface area. This clearly demonstrates that copper has penetrated into the silicon under mechanical stress.

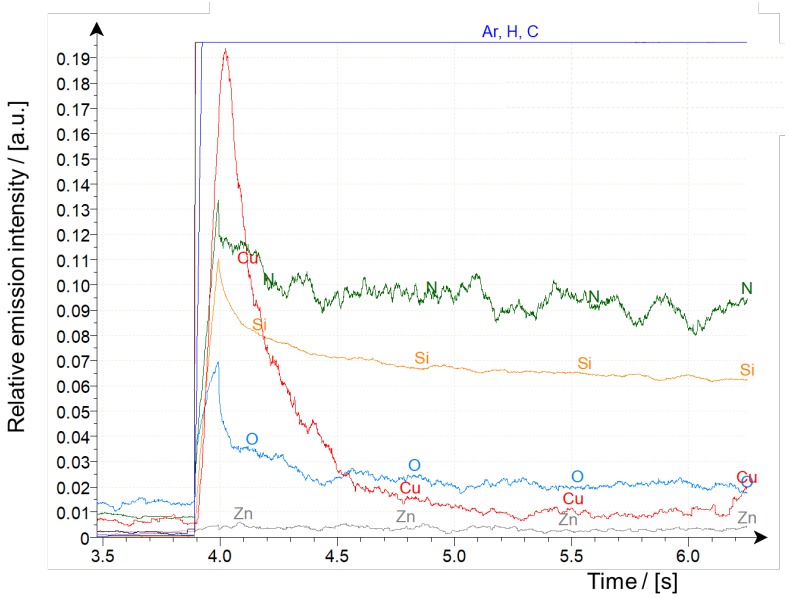

Figure 3: GD-OES depth profile analysis for a Si wafer treated with a brass polishing wheel in a $CuSO_4$ solution.

Figure 3 shows the depth profile after treatment the silicon surface with the brass polishing wheel immersed in a copper solution. Although the profile of the copper emission intensity also shows a very strong surface enrichment of copper, the drop over the erosion time occurs much more rapidly than in Figure 2 indicating a lower penetration depth. No significant enrichment of zinc is observed, and the presence of oxygen appears to be concentrated very close to the surface. The differences between Figure 2 and Figure 3 indicate that, in the presence of the aqueous solution, the copper penetrates less deeply into the silicon and less oxidation

in the topmost surface region only. This suggests that the aqueous solution leads to better heat distribution during the mechanical treatment, which attenuates the local temperature rise. Thus, in addition to mechanical pressure, the influence of temperature is particularly decisive for the penetration and diffusion of the copper.

In conclusion, the presence of metallic copper and significant mechanical stress load is necessary for the diffusion of copper into silicon. In order to determine the penetration depth of the copper within the silicon particles, the kerf was partially etched stepwise using a very slow-etching HF-HNO_3 mixture. A after washing and drying, the material was cleaned again with concentrated HNO_3 to remove metallic copper deposited from the surface. After washing and drying again, the material was completely dissolved in an HF/HNO_3 mixture and analyzed by ICP-OES (Rietig and Acker, 2017). The quantitatively determined silicon content was used to calculate the amount of silicon removed. A total of 6 etching steps were performed, and 7%, 15%, 20%, 23%, 34%, and 49% of the silicon was dissolved.

The black dotted curve in Figure 4a shows the particle size distribution of the as-received kerf. Based on that curve, the volume loss of total silicon by stepwise etching was converted, in average, into a uniform thickness removal for silicon particles of all sizes resulting in particles of lesser diameter. The calculated solid curves in Figure 4a represent the loss of volume in each particle size fraction and in each etching step; which is more instructive than a plot of the obtained particle size distribution after each etching step. Figure 4a shows that particles smaller than 2 µm faces the highest volume loss, while particles larger than 5 µm show virtually no loss in volume.

Figure 4b shows the copper concentrations in the etched kerf samples with increasing averaged removal. The trend follows a typical concentration profile of solid-state diffusion according to the square root law (Ward *et al.*, 1982; Hong *et al.*, 1991). Clearly, the top 50 nm layer of the silicon particles contains the most copper. This value is halved within a further 50–100 nm of removal. A minimum of 1 ppm can be achieved removing of 350 nm silicon. However, such a procedure cannot be recommended, because the silicon loss amounts to nearly 50%.

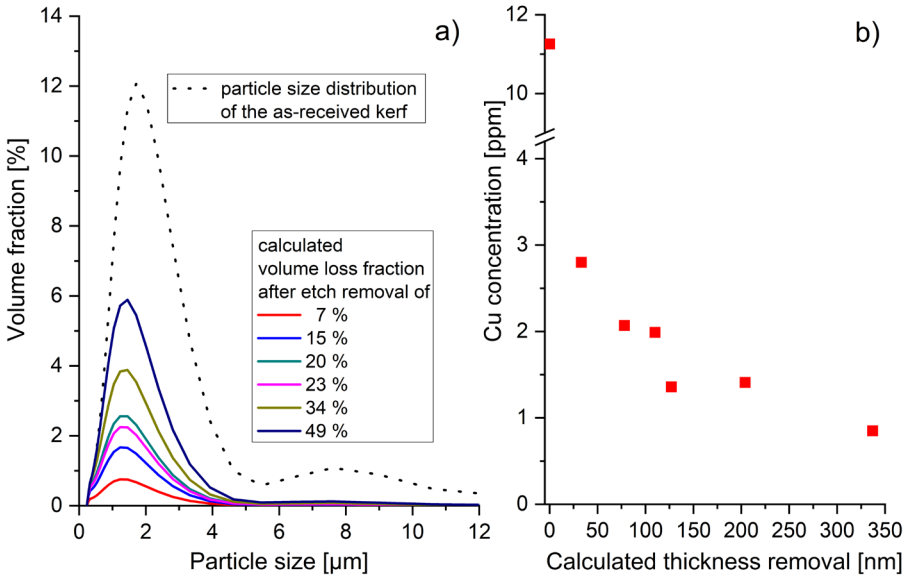

Figure 4: a) Particle size distribution calculated from the measured particle size distribution (black curve) as etching removal increases. b) Copper content in the kerf after layer-by-layer dissolution of the silicon.

2.4 Development of a multi-stage acid treatment process

Preliminary studies show that the efficient removal of metallic impurities requires a multi-step treatment. This has led to a sequence of acid treatments that has proven to be particularly effective. The first step involves treatment with nitric acid to remove surface metal impurities, particularly copper, without causing redeposition. The second step involves treatment with a low-concentration hydrofluoric acid solution to primarily remove oxide layers on the silicon particles. The third step involves treatment with hydrochloric acid to remove residual metals located within or beneath the oxide layer on the silicon particles that have not yet been completely dissolved by nitric and hydrofluoric acid. Three concentrations were selected for each acid: 5, 15, and 30% (w/w) for nitric acid; 1, 2, and 4% (w/w) for hydrofluoric acid; and 5, 15, and 30% (w/w) for hydrochloric acid. The concentration of hydrofluoric acid was set very low to minimize silicon loss as much as possible.

Figures 5 and 6 provide examples comparing the final removal efficiency of three consecutive treatment steps, which differ in the concentration of HNO_3 in the first treatment step at 15% (Figure 5) and 30% (Figure 6). It should be noted that the impurity elements are present in very different initial concentrations (Table I).

All results show (even with an initial treatment step using 5% HNO_3) that the elements Al, Ca, Ni, and Zn are removed almost completely. The removal of Mg always requires the highest acid concentrations to achieve a removal of more than 85%. The reason for the difference between Ca and Mg—namely, that Mg is not nearly completely removed under the same conditions—is unknown. In contrast, a clear trend can be observed for iron. Removal reaches its respective maximum value when the highest HCl concentration is used in the final step. The residual iron levels range from 81 ppm (5% HNO_3, 1% HF, 5% HCl) to 6 ppm (5% HNO_3, 4% HF, 30% HCl), making it the second most significant impurity in the leached kerf.

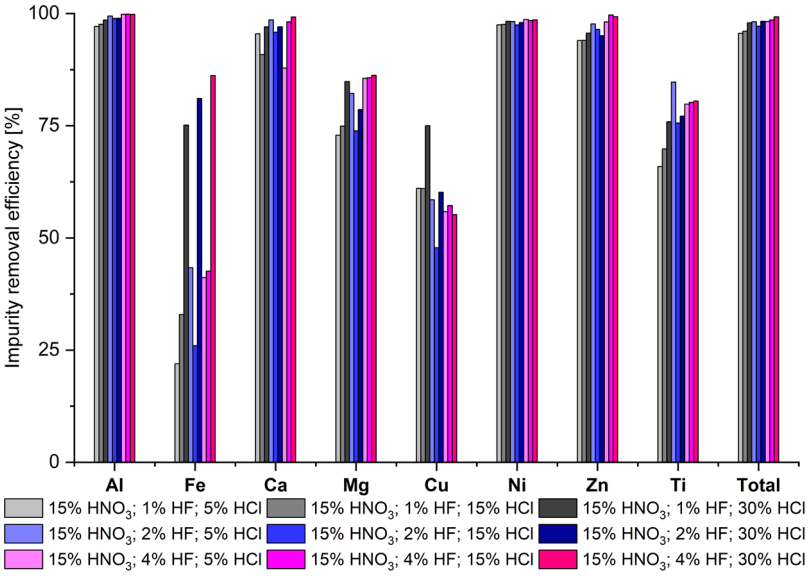

Figure 5: Cleaning efficiency following treatment with 15% HNO_3 in the first step, followed by 1% to 4% HF in the second step and 5% to 30% HCl in the third step.

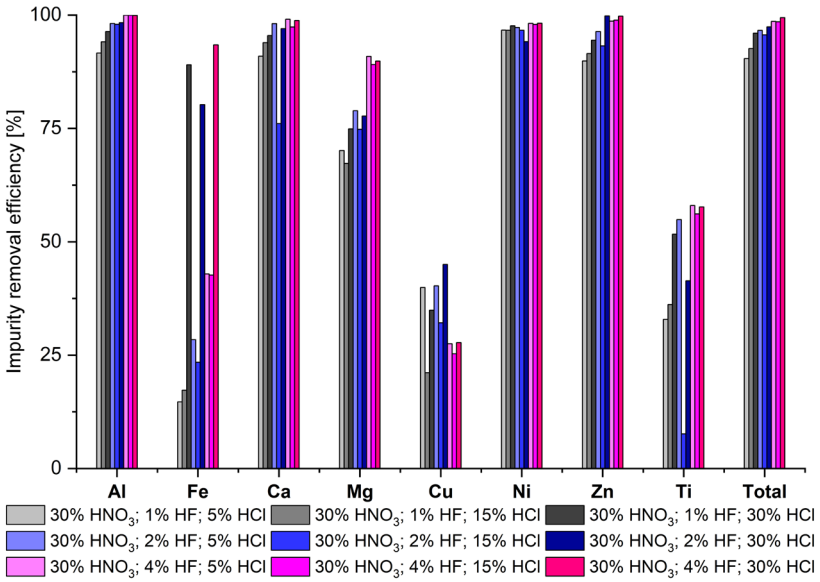

Figure 6: Cleaning efficiency following treatment with 30% HNO_3 in the first step, followed by 1% to 4% HF in the second step and 5% to 30% HCl in the third step.

Titanium is present in the kerf only at a very low initial concentration of 1.3 ppm. The higher the acid concentrations, the more titanium dissolves, which results in the lowest residual levels—between 0.2 ppm and 0.4 ppm—in the series using 30% HNO_3 in the first treatment step. Thus, titanium contributes only minimally to the remaining impurities in the treated kerf.

Copper, on the other hand, exhibits more complex behavior. The treatment series using 5% HNO_3 in the first treatment step achieve a reduction of between 20% and 45%. Removal efficiency increases with acid concentration and, with 30% HNO_3 in the first treatment step, reaches values between 47% and 75%, resulting in final copper levels between 4.4 ppm and 5.9 ppm. Copper and nickel thus rank third in terms of their contribution to contamination.

To further illustrate the purification effect of the acid combinations, Figure 7 shows the absolute concentrations of several selected elements—nickel, iron, and copper—for each individual step of treatment, including the results from the series using 5% HNO_3 in the first treatment step.

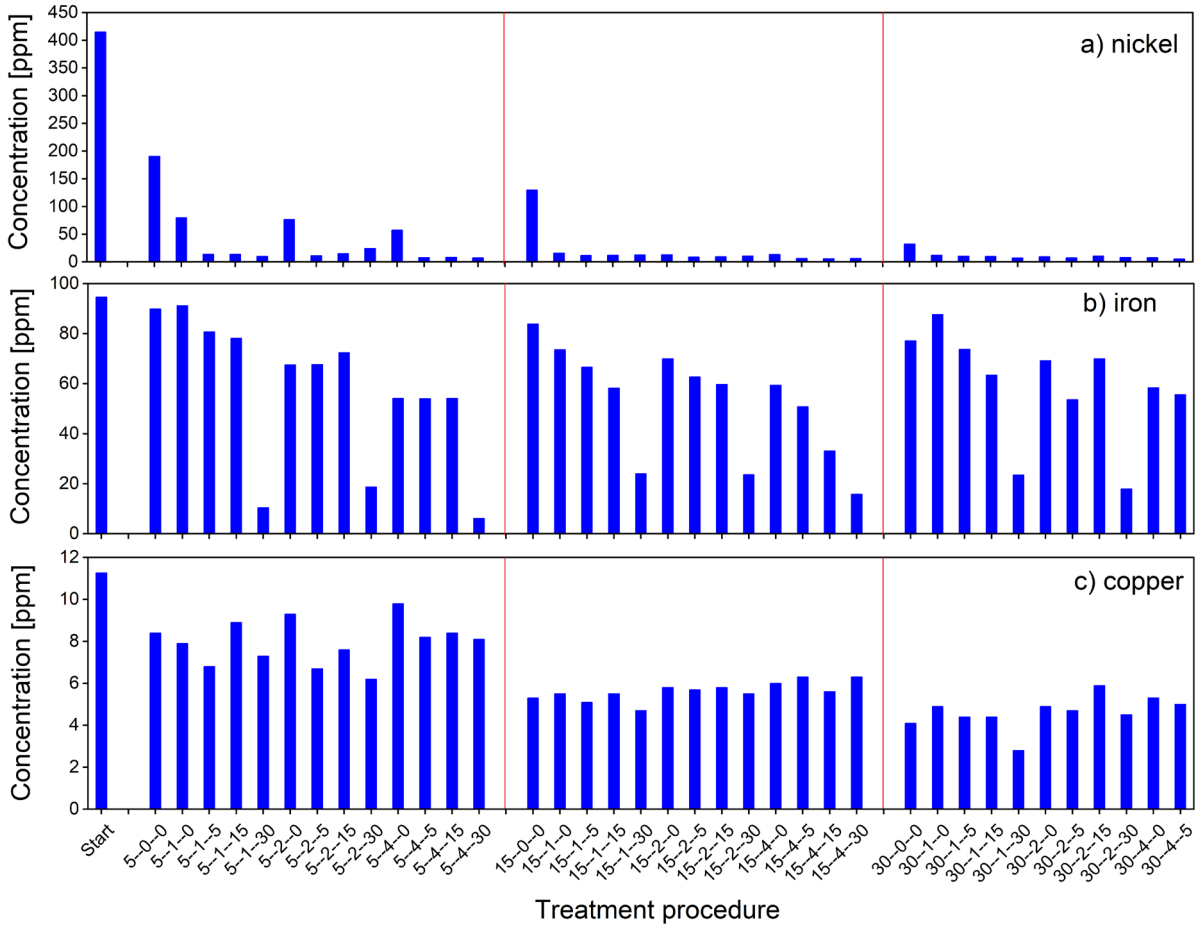

Figure 7. Element contents for a) nickel, b) iron, and c) copper according to the respective treatment steps. The first number indicates the concentration of HNO_3 (in %(m/m)) in the first treatment step, the second number indicates the concentration of HF (in %(m/m)) in the second treatment step, and the third number indicates the concentration of HCl (in %(m/m)) in the third treatment step.

Nickel (Figure 7a) exhibits the ideal typical trend of decreasing concentrations with each treatment step. HNO_3 in the first step of treatment and with increasing concentration removes always the majority of the present nickel contaminations. Only for 5% HNO_3 the subsequent acid treatments still play a role in nickel removal; however, their effect diminishes starting at 15% HNO_3. In fact, HNO_3 is thus the most important acid component for the removal of nickel.

In the case of iron (Figure 7b), the highest purifying effect comes from HCl, whereas high-concentration hydrochloric acid has the highest removal effect. Treatment with HNO_3 in the first step does not lead to a significant reduction in the iron concentration. However, as higher the HNO_3 as lower is the removal efficiency. It is interesting to note, that the removal by hydrochloric acid is less effective with higher the concentration of HNO_3 in the first treatment step. It can be assumed that HNO_3 leads to passivation of the iron, which is less pronounced at low HNO_3 concentrations. Hydrofluoric acid treatment does not appear to have any significant effect.

The most interesting behavior shows copper (Figure 7c). The concentration of HNO_3 in the first treatment step plays the most significant role in copper removal; the higher the concentration, the lower the residual copper content. HNO_3 treatment dissolves the copper impurities that are accessible to the acid. The subsequent treatment steps show only a marginal effect, because the remaining copper has diffused into the silicon. Copper shows an interesting effect that is also seen for the chemical cleaning of other materials for elements in low

concentrations. When kerf is treated with HF, the copper concentration remains virtually unchanged or even increases slightly, whereby the increase corresponds to an increase of the HF concentration. HF treatment leads to the removal of the oxide layer from the silicon particles that therefore lowers the mass of the remaining silicon; i.e. the total mass of the sample after HNO_3 treatment is higher than after HF treatment due to oxide removal. After complete digestion with HF/HNO_3 the quantified amount of copper is divided by a lower value for the mass of silicon resulting in a slightly higher Cu concentration after HF treatment compared to that after HNO_3 treatment. However, it cannot be ruled out that a fraction of copper may be trapped within the oxide layer and partially dissolved by HF—may have been redeposited.

Overall, it can be stated that, the treatment steps examined achieved a silicon purity of 99.947% for the sequence 5% HNO_3 - 1% HF - 5% HCl and in the best-case scenario, 99.996% for the sequence 30% HNO_3 - 4% HF - 30% HCl (Table I).

3. CONCLUSIONS

The use of diamond wire saws with brass-bonded diamond particles leads to the introduction of copper into the resulting silicon kerf during silicon sawing. The challenge with copper-containing kerf is finding a suitable use for it. Since copper in silicon leads to deep electronic defects, direct further processing—such as melting crystalline silicon for photovoltaic applications—is not recommended without prior pretreatment to remove the copper. Possible approaches could involve using it as a copper-containing feedstock for the production of methylchlorosilanes. What is interesting, however, is a potential application for producing anode material for lithium-ion batteries. Highly interconnected hollow Si–Cu alloy nanotubes can serve as high-capacity and self-conductive anode structures with robust mechanical support in lithium ion batteries (Song *et al.*, 2016).

To determine the cause of the copper content in the silicon, the process of mechanical force exerted by copper-containing material on a silicon surface was simulated under various conditions, and the penetration behavior of the copper into the silicon was determined using GD-OES depth profile analysis. The basic prerequisite for copper contamination is mechanical contact between the copper-containing material and the silicon; dissolved copper ions play no role. The layer-by-layer etching of the silicon particles indicates that the copper diffuses into the silicon, with its concentration decreasing with depth according to the square root law. It appears, that the driving force for copper diffusion is a local temperature increase at the silicon/copper interface initiated by the mechanical load and the resulting fracture formation. The presence of a cooling medium is able to dampen this effect, however, not able to prevent it. Copper diffusion into silicon is known to start at temperatures as low as 200 °C (Ward *et al.*, 1982; Hong *et al.*, 1991), however, the local temperatures are apparently not high enough to form copper silicide phases. Therefore, the copper that has penetrated is likely present as a solid solution of copper in silicon and is consequently not attacked by acids. As a result, a further reduction in the copper concentration can only be achieved by dissolving a significant portion of the silicon—approximately 50%.

The wet chemical treatment regimens examined demonstrate the contradictory behavior of the metallic impurities in the kerf when exposed to various acids, so that a combined approach using different acids is necessary if high purity is to be achieved through wet chemical treatment steps alone. If only acid treatment at room temperature is considered, a regime based on an HNO_3-HF-HCl treatment using moderate acid concentrations for both HNO_3 and HCl proves to be the most efficient of all tested variants. In the present investigations, it was

thus possible to achieve a purity of 99.996% Si with a final copper concentration of 5.0 ppm starting from a kerf with a silicon content of 99.443% Si.

4. REFERENCES

Hong S.Q., Comrie C.M., Russell S.W., and Mayer J.W. 1991. Phase formation in Cu-Si and Cu-Ge. *Journal of Applied Physics*, Vol.70, pp.3655-3360. https://doi.org/10.1063/1.349213

Kong J., Xing P., Liu Y., Wang J., Feng Z., and Luo X. 2019. An Economical Approach for the Recycling of High-Purity Silicon from Diamond-Wire Saw Kerf Slurry Waste. *Silicon*, Vol.11, pp.367–376. https://doi.org/10.1007/s12633-018-9889-x

Kumar A., and Melkote S.N. 2018. Diamond wire sawing of solar silicon wafers: A sustainable manufacturing alternative to loose abrasive slurry sawing. *Procedia Manufacturing*, Vol.21, pp. 549-566. https://doi.org/10.1016/j.promfg.2018.02.156

Li X., Lv G., Ma W., Li T., Zhang R., Zhang J., Li S., and Lei Y. 2022. Review of resource and recycling of silicon powder from diamond-wire sawing silicon waste. *Journal of Hazardous Materials*, Vol.424, p.127389. https://doi.org/10.1016/j.jhazmat.2021.127389

Li A., Hu S., Zhou Y., Wang H., Zhang Z., and Ming W. 2023. Recent advances in precisions diamond wire sawing monocrystalline silicon. *Micromachines*, Vol.14, Issue 8, p.1512. https://doi.org/10.3390/mi14081512

Lottspeich L., Müller P., and Kaden T. 2018. Metal contamination of silicon wafers in diamond wire sawing processes depending on the sawing parameters. *AIP Conference Proceedings*, Vol.1999, 140003. https://doi.org/10.1063/1.5049342

Möller H. J. 2004. Basic mechanisms and models of multi-wire sawing. *Advanced Engineering Materials*, Vol.6, pp.501–513. https://doi.org/10.1002/pssa.200564508

Rietig A., and Acker J. 2017. Development and validation of a new method for the precise and accurate determination of trace elements in silicon by ICP-OES in high silicon matrices. *Journal of Analytical Atomic Spectrometry*, Vol. 32, pp.322–333. http://dx.doi.org/10.1039/C6JA00241B

Schönekerl S., and Acker J. 2020. The kinetics and stoichiometry of metal cation reduction on multi-crystalline silicon in a dilute hydrofluoric acid matrix. *Nanomaterials*, Vol.10, Issue 12, p.2545. https://doi.org/10.3390/nano10122545

Song H., Wang H.X., Lin Z., Jiang X., Yu L., Xu J., Yu Z., Zhang X., Liu Y., He P., Pan L., Shi Y., Zhou H., and Chen K. 2016. Highly Connected Silicon–Copper Alloy Mixture Nanotubes as High-Rate and Durable Anode Materials for Lithium-Ion Batteries. *Advanced Functional Materials*, Vol.26, pp. 524–531. https://doi.org/10.1002/adfm.201504014

Ward W.J., and Carroll K.M. 1982. Diffusion of Copper in the Copper-Silicon System. *Journal of the Electrochemical Society*, Vol.129, pp.227-229. https://doi.org/10.1149/1.2123764

Würzner S., Herms M., Kaden Th., Möller H.-J., and Wagner M. 2017. Characterization of the diamond wire sawing process for monocrystalline silicon by Raman spectroscopy and SIREX polarimetry. *Energies*, Vol. 10, 414. https://doi.org/10.3390/en10040414

Xiong, B., Han, S., Yang, S., Xie, K., Wei, K., and Ma, W. 2024. Review of silicon recovery from diamond wire saw silicon powder waste based on hydrometallurgical process. *Molecules*, Vol.29, p.5645. https://doi.org/10.3390/molecules29235645

Jörg Acker

Professor, Chair and Head of Department of Physical Chemistry, Brandenburg University of Technology Cottbus-Senftenberg, Germany

He earned his Ph.D. (1999) and completed his habilitation (2004) at the Technical University of Freiberg, focusing on metal-catalyzed reactions of chloro- and methylchlorosilanes. After holding positions at Princeton University and the Leibniz Institute for Solid State and Materials Research in Dresden, he became a full professor of physical chemistry at the Brandenburg University of Technology. He continues to work in various areas of silicon chemistry, although for the past 14 years his main research topics have been lithium-ion battery recycling, spectroscopy, microscopy, and chemical analytics.